

Idiosyncrasies of Physical Vapor Deposition Processes from Various Knudsen Cells for Quinacridone Thin Film Growth on Silicon Dioxide

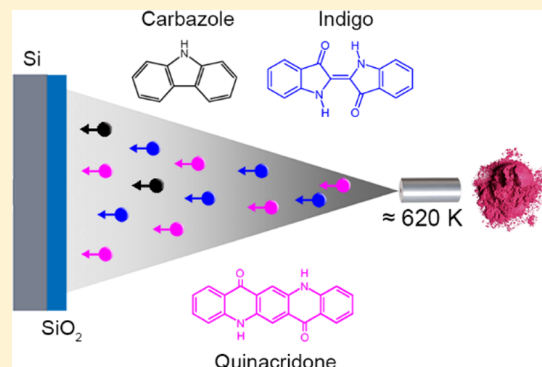
Boris Scherwitzl,[†] Christian Röthel,^{†,‡} Andrew O. F. Jones,[†] Birgit Kunert,[†] Ingo Salzmann,[§] Roland Resel,[†] Günther Leising,[†] and Adolf Winkler^{*,†}

[†]Institute of Solid State Physics, Graz University of Technology, Petersgasse 16, A-8010 Graz, Austria

[‡]Institute of Pharmaceutical Sciences, Department of Pharmaceutical Technology, Karl-Franzens Universität Graz, Universitätsplatz 1, A-8010 Graz, Austria

[§]Institut für Physik, Humboldt-Universität zu Berlin, Brook-Taylor-Straße 6, 12489 Berlin, Germany

ABSTRACT: Thin films of quinacridone deposited by physical vapor deposition on silicon dioxide were investigated by thermal desorption spectroscopy (TDS), mass spectrometry (MS), atomic force microscopy (AFM), specular and grazing incidence X-ray diffraction (XRD, GIXD), and Raman spectroscopy. Using a stainless steel Knudsen cell did not allow the preparation of a pure quinacridone film. TDS and MS unambiguously showed that in addition to quinacridone, desorbing at about 500 K (γ -peak), significant amounts of indigo desorbed at about 420 K (β -peak). The existence of these two species on the surface was verified by XRD, GIXD, and Raman spectroscopy. The latter spectroscopies revealed that additional species are contained in the films, not detected by TDS. In the film mainly composed of indigo a species was identified which we tentatively attribute to carbazole. The film consisting of mainly quinacridone contained in addition p-sexiphenyl. The reason for the various decomposition species effusing from the metal Knudsen cell is the comparably high sublimation temperature of the hydrogen bonded quinacridone. With special experimental methods and by using glass Knudsen-type cells we were able to prepare films which exclusively consist of molecules either corresponding to the β -peak or the γ -peak. These findings are of relevance for choosing the proper deposition techniques in the preparation of quinacridone films in the context of organic electronic devices.



I. INTRODUCTION

Organic thin films have attracted considerable interest in the recent past, most notably due to new manufacturing steps and the possibility to create ultrathin and lightweight devices with extreme bending stability,^{1–3} that are very promising in the field of organic electronics.⁴ Through observing current and projected environmental problems, the aspect of biodegradability has progressively risen in importance and might now be the most crucial argument in pursuing research in the field of organic semiconductors.^{5,6} Quinacridone (QA, $C_{20}H_{12}N_2O_2$) and other high-performance organic pigments have particularly been in the focus of attention, attributable to the formation of intermolecular hydrogen bonds.⁷ Quinacridone, also known as linear trans-quinacridone,⁸ has a molecular mass of 312.32 amu and was first synthesized 1935 by Liebermann et al.⁹ The discovery of its polymorphism and more efficient synthesis methods years later^{10–13} consequently led to simpler synthesis routes and has provoked considerable interest in the scientific community ever since.¹⁴ Organic pigments are, contrary to organic dyes, generally insoluble. Current literature research unveils a formidable amount of works elucidating how adding various kinds of solubilizing groups to the quinacridone molecule gave rise to a number of new applications, most

notably as photodetectors¹⁵ and both donor and acceptor molecules in organic solar cells.^{16–18} Their general insolubility, in turn, makes physical vapor deposition the method of choice for manufacturing thin layers, which is in the focus of the present publication. It is well-known that preparation parameters such as substrate temperature, substrate conditions, base pressure, and deposition rate determine the morphology and hence the electronic structure and optical properties of thin films grown by vapor deposition.^{19–22} Despite recent reports of air-stable quinacridone field-effect transistors with relatively high carrier mobilities of $0.2 \text{ cm}^2/(\text{V s})$,²³ there is still a lack of knowledge concerning the kinetics of vacuum deposition and film formation on industrially relevant silicon dioxide substrates. Comparable investigations on the kinetics of adsorption, layer growth and desorption exist for a number of organic molecules (e.g., pentacene on SiO_2 ²⁴ and rubicene on SiO_2 ²⁵), while the focus has only recently shifted to H-bonded semiconductors.^{26–29}

Received: April 29, 2015

Revised: August 11, 2015

Published: August 17, 2015

In this work, we focus on the growth and desorption behavior of quinacridone on/from SiO_2 substrates under ultrahigh vacuum conditions and report multiple collision-induced thermal decomposition processes both within the Knudsen evaporation cells and on the substrate surface. Thermally induced cracking leads to a formation of multiple, typically undefined fragmentation products that may influence, e.g., transistor characteristics. It is therefore of high importance to study molecular decomposition and the underlying driving forces on a chemical level and also to evaluate its occurrence and magnitude upon variation of the deposition methods. Complementing the in situ methods of thermal desorption spectroscopy (TDS) and Auger electron spectroscopy (AES), ex-situ analysis by atomic force microscopy (AFM), specular X-ray diffraction (XRD), grazing incidence X-ray diffraction (GIXD), and Raman spectroscopy were used to address this issue.

II. EXPERIMENTAL SETUP

For all of our experiments sublimation purified quinacridone, provided by Tokyo Chemical Industry with a purity of >99%, was used. Typically, the material was deposited, after proper outgassing, i.e., the evaporation of smaller and more volatile impurity molecules during the heating process, via physical vapor deposition from a stainless steel Knudsen cell heated to about 620 K. The inner diameter of the cell was 7 mm, the length was 20 mm, and the effusion hole diameter was 1 mm (see insert in Figure 1). For several experiments it was

thermal desorption measurements. Detailed information on the experimental setup is given in previous publications.^{25,28} The deposition process was conducted with a typical deposition rate of 105 ng/(min·cm²), equivalent to 0.7 nm/min and controlled by a quartz microbalance, which could be placed intermittently at the sample position. Deposition and in situ characterization were carried out in an ultrahigh vacuum system housing a Pfeiffer QMS 200 mass spectrometer and a Staib Instruments Auger electron analyzer. The base pressure of the unbaked UHV chamber was typically 6×10^{-9} mbar. Furthermore, the whole sample stage was LN₂ cooled to 200 K during film deposition, if not stated otherwise.

An analysis of the chemical composition of the untreated substrate surface via AES revealed silicon and oxygen peaks originating from the substrate, with a slight carbon contamination on top. This carbon signal increased slightly as a consequence of repeated adsorption–desorption cycles. Such a carbon covered SiO_2 surface was used for the described experiments. An Auger analysis of vapor deposited quinacridone films showed the expected carbon, nitrogen and oxygen signals. Unfortunately, it was not possible to perform continuous Auger surveillance during different stages of the film growth process, due to the destructive behavior of the electron beam on the organic films. After material deposition the samples were placed in front of a quadrupole mass spectrometer (QMS) tuned to typical cracking masses of quinacridone, i.e., either to 128 or 76 amu. Continuous heating with a heating rate of 1 K/s subsequently caused material desorption and made for a convenient way to study film characteristics, growth, and desorption behavior as well as desorption order and activation energies for desorption.³⁰ In this context, we have to emphasize that the sample temperature, as measured at the back side of the silicon wafer, is not the same as on the SiO_2 surface, due to the bad heat conductivity in silicon and SiO_2 , as well as due to a thermal bridge at the interface between the Si wafer and the stainless steel heating plate. However, a temperature correction can be made by comparing the multilayer desorption peak from the sample with that from the metal clamps, the temperature of which can be considered to be equal to the measured temperature. More details on the conducted temperature correction can be found elsewhere.³¹ When analyzing TD spectra of organic molecules with a QMS, cracking of the molecules in the ionization chamber of the spectrometer is unavoidable. This is due to electron impact induced fragmentation during the ionization process. Therefore, the cracking pattern depends on several QMS setting parameters. The measured cracking masses should not be mixed up with possible decomposition products entering the ionization chamber of the QMS after desorption from the surface.

Ex-situ studies of film morphologies and structures were done utilizing an atomic force microscope (Nanosurf Easyscan 2) in tapping mode employing PPP-NCLR-50 silicon tips from NANOSENSORS. Specular X-ray diffraction (SXRD) measurements have been performed on a PANalytical EMPYREAN diffractometer fitted with a Cu sealed tube and a multilayer mirror ($\lambda = 1.54 \text{ \AA}$) on the primary side. The secondary side was equipped with a slit system and intensities were recorded using a PANalytical PIXcel detector in 1D mode. Grazing incidence X-ray diffraction (GIXD) measurements were conducted at the KMC-2 beamline at BESSY II (Berlin, Germany) using X-rays with a wavelength of 1.00 \AA and a 2D cross-wire detector (BRUKER).³² An incident angle of $\alpha_i =$

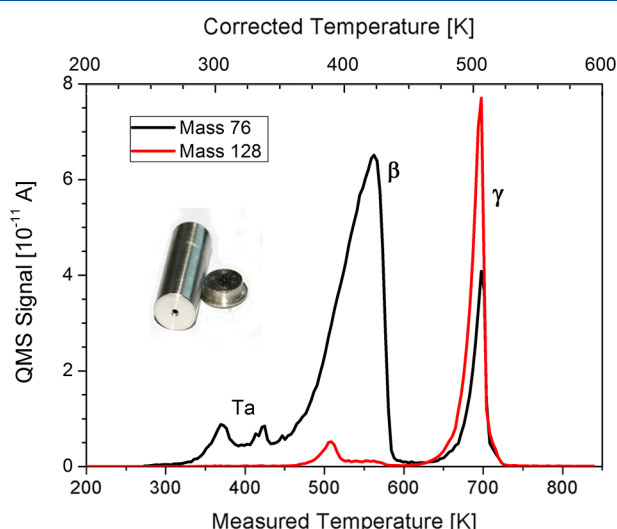


Figure 1. Thermal desorption spectra for cracking masses of 76 amu (black) and 128 amu (red) of a 4.25 nm thick film which was grown on carbon covered silicon dioxide by evaporation of quinacridone from a stainless steel cell. Adsorption temperature $T_{ad} = 200 \text{ K}$, deposition rate $A = 0.7 \text{ nm/min}$, heating rate $\beta = 1 \text{ K/s}$. The small peaks at 310, 340, and 380 K stem from desorption from the Ta mounting clamps.

necessary to switch to a glass Knudsen cell or other glass evaporation sources, explained in more detail below. As substrate material, silicon dioxide with a nominal thickness of 150 nm, that has been thermally grown on 0.67 mm thick Si(001) wafers (Siegert Wafer GmbH), was used. The $1 \times 1 \text{ cm}^2$ large substrates were mounted onto a stainless steel heating plate via four tantalum clamps. Attached to the steel plate are two tantalum wires for resistive heating and a Ni/NiCr thermocouple to complete the feedback loop, necessary for

0.13° was chosen to enhance the scattered intensities of the adsorbate. Reciprocal space maps were calculated with the Xray Utilities library for Python.³³ The micro-Raman experiments were performed with a HeCd-laser excitation wavelength of 325 nm on a LABRAM HR-800 (HORIBA Jobin Yvon) Raman-spectrometer using gratings of 2400 lines/mm and providing a spectral resolution of 3.92 cm^{-1} . The detection system was a liquid-nitrogen-cooled CCD spectrometer.

III. RESULTS AND DISCUSSION

A. Adsorption and Desorption of Quinacridone and Its Decomposition Products on/from SiO_2 . Initially, thermal desorption experiments were carried out after physical vapor deposition of quinacridone on carbon covered SiO_2 from a metal Knudsen cell. The thermal desorption spectra of a 4.25 nm thick quinacridone film yielded a single desorption peak at about 500 K (denoted γ , see red line in Figure 1) when the QMS was tuned to a cracking mass of 128 amu. The cracking fragment at 128 amu was chosen because it is very prominent in the quinacridone cracking pattern³⁴ and showed a reasonably good signal-to-noise ratio. Experimental limitations did not allow detecting the main mass of quinacridone or any other fragments higher than 200 amu. If there were only a single molecular species present on the surface, as one might assume from the red curve in Figure 1, then the choice of cracking mass should have no significant influence and spectra for different cracking masses should be comparable. However, surprisingly, when tuning the QMS to the cracking mass 76 amu, a second peak at about 420 K (denoted β -peak, black line in Figure 1) appeared, in addition to the expected peak at 500 K. This points toward the presence of a second, weakly bonded type of molecules with a different cracking pattern and, hence, a different desorption behavior. Indeed, a full mass scan between 35 and 150 amu during desorption of the β and γ -peak, respectively, clearly shows different cracking patterns (Figure 2). Therefore, we can deduce the existence of two distinct and chemically different thin-film species on the surface, despite the fact that only purified quinacridone was present in the Knudsen cell. The γ -peak and its cracking pattern are in good agreement with literature data of quinacridone,³⁴ and we therefore assume that it corresponds to thermal desorption of pure quinacridone. This assumption is supported by several spectroscopic analyses, as will be shown below. Combining the cracking pattern of the β -peak with specular X-ray diffraction, Raman spectroscopy and GIXD allowed us to match this peak with indigo (IN, $\text{C}_{16}\text{H}_{10}\text{N}_2\text{O}_2$).³⁵ Indeed, multiple spectroscopic observations of a film corresponding to the β -peak agree reasonably well with data from an earlier publication describing the growth and desorption behavior of pure indigo films that were grown on SiO_2 under identical conditions.²⁸ However, the spectroscopic data hint at the existence of an additional type of molecules in this film, which we could identify to be carbazole (CA, $\text{C}_{12}\text{H}_9\text{N}$).³⁶

At this point, the question arises whether indigo is generated on the silicon dioxide surface during heating of a pure quinacridone film or whether this type of molecules is already effusing from the stainless steel Knudsen cell. To address this issue, we have performed the following experiments: After the growth of a thin film with the described physical vapor deposition from the stainless steel Knudsen cell, a second sample holder with an identical Si/SiO_2 wafer, held at room temperature, was put in front of the primary sample. Heating this primary sample to 425 K exclusively caused the molecules

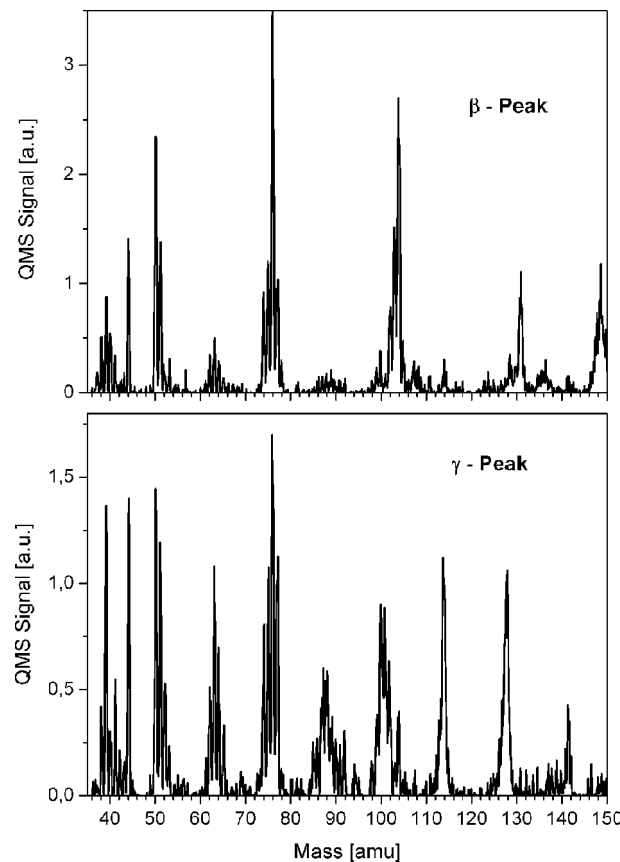


Figure 2. Accumulated mass spectra (cracking spectra) of the desorption flux in the range of 350–450 K (β -peak) and 470–530 K (γ -peak). Sweep rate: 0.2 s/amu. A 3 nm thick film, prepared by evaporation of quinacridone from a stainless steel Knudsen cell was used for this experiment. Heating rate: 1 K/s, Adsorption temperature: 200 K.

corresponding to the β -peak to desorb while the more strongly bonded quinacridone remained. The employed geometry (1.0 cm distance between the two 1 cm^2 large samples, assuming a cosine desorption distribution) allowed about 1/3 of the desorbed molecules to readsorb on the stationary sample, which turned out to be a convenient way to create films with solely weakly bonded indigo and/or other decomposition molecules (β -peak). After breaking the vacuum this stationary sample was installed on the heatable sample holder and a TDS was performed as soon as UHV conditions were reached. The desorption spectrum of this film was similar in shape to the original β -peak, demonstrating that this molecular species remains unchanged during the described readsorption and subsequent desorption.

Applying a similar experimental procedure, material corresponding to the γ -peak was deposited on the stationary sample and a TDS was performed after venting and re-evacuation. In this case, solely the γ -peak appeared in the desorption spectrum, confirming that the β -peak is not a result of quinacridone decomposition during sample heating. Thus, the indigo observed in the desorption spectrum (Figure 1) must have originated from the stainless steel Knudsen cell. Indeed, a full mass spectrum between 35 and 200 amu of the deposition flux leaving the metal Knudsen cell (see Figure 3) confirmed the existence of prominent cracking fragments from both indigo (β -peak) and quinacridone (γ -peak) molecules. Thermal

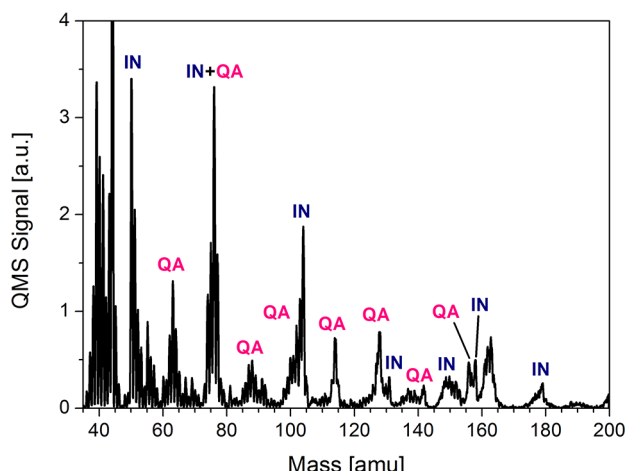


Figure 3. Cracking spectrum of the stainless steel Knudsen cell deposition flux. Knudsen cell temperature: 650 K.

decomposition (pyrolysis), dissociation and isomerization processes involving collisions of organic molecules with hot surfaces are commonly observed and well characterized in the field of organic chemistry.^{37,38} Apparently, quinacridone seems to be particularly prone to such decomposition processes, due to its high sublimation temperature.³⁹ However, only sparse reports exist involving cracking and/or restructuring of chemical bonds with the subsequent formation of new and stable molecules for quinacridone-based and other H-bonded materials. Haucke et al.⁴⁰ described a smooth and homogeneous transition from indigo to epindolidione in the vapor phase, if the former is heated to 733 K under vacuum conditions. Berg et al.²⁶ observed decreasing mobilities for quinacridone organic field-effect transistors grown in vacuum after repeated temperature gradient sublimation preparation circles.

After having verified that a decomposition process takes place in the stainless steel Knudsen cell the question arises as to the quantitative ratio of the effusing molecules, corresponding to the β - and γ -peak. Despite the fact that both species exhibit common cracking masses (e.g., 76 amu), one has to be aware that the intensities of the different desorption peaks depend on the detailed measurement conditions and no statements can be made on the actual distribution and relative amount of the molecules on the samples. To address this issue, we have performed AFM measurements on films prepared with the method described above, consisting either of material corresponding to the β or γ -peak, respectively. Evaluation of the cross sections of the island-like films allowed a quantitative determination of the effusion rates. A flux ratio of $63 \pm 5\%$ indigo to $37 \pm 5\%$ quinacridone was obtained. A detailed description of the calibration procedure for quinacridone decomposition in the stainless steel Knudsen cell will be given in a future publication. All given mean thickness values in this publication correspond to the total amount of adsorbed material, hence including both molecules. The molecular ratio given above should therefore be taken into account if the two types of molecules were to be analyzed separately.

B. Influence of the Knudsen Cell Type on the Evaporation of Quinacridone. In a first attempt to quantify and describe the chemical cracking process and to confirm the coexistence of different types of molecules on the surface, despite the fact that only purified quinacridone is present in the

Knudsen cell, the deposition process was repeated with various Knudsen cells and different evaporation sources. In order to check the purity of the quinacridone source material and to, therefore, rule out possible contaminations, a 18 nm thick quinacridone film was grown on a silicon dioxide sample via Langmuir evaporation from an open quartz glass tube (see inset in Figure 4) in a separate vacuum chamber. The sample was

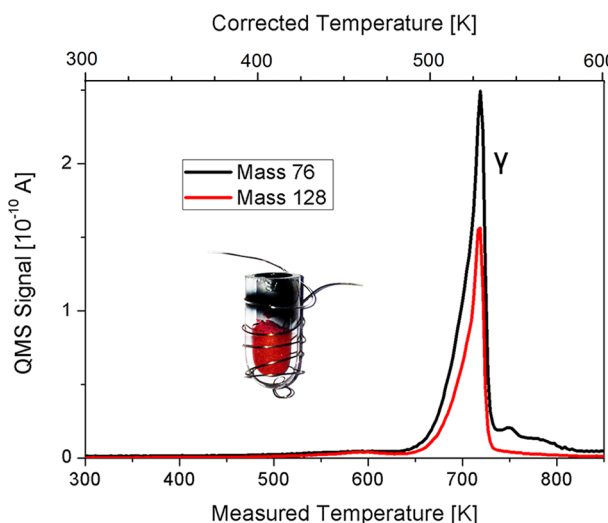


Figure 4. Thermal desorption spectrum for an 18 nm thick quinacridone film deposited from a glass evaporation cell (Langmuir evaporation). Substrate temperature: 300 K.

then again installed in the UHV chamber and analyzed via thermal desorption. As shown in Figure 4, only the γ -peak appears in the desorption spectrum, indicating that the employed material is indeed pure and that no material decomposition occurs in that case. In the case of Langmuir evaporation (or free evaporation)⁴¹ the sublimed molecules can be deposited at the substrate surface without any further collision in between. Contrary, in the evaporation from a Knudsen cell the sublimed molecules hit many times the inner cell wall before they leave the small effusion hole. For our particular stainless steel Knudsen cell dimensions, a distance of 5 cm between sample and Knudsen cell orifice and a typical deposition flux of $105 \text{ ng}/(\text{min cm}^2)$ we calculate that a sublimed particle hits the inner walls about 400 times before escaping through the effusion hole. This corroborates our assumption of a thermally activated decomposition process within the metal Knudsen cell.

As a next step, it comes to answer the question whether the decomposition of quinacridone occurs due to a possible catalytic behavior of stainless steel or whether it can be reproduced in other Knudsen-like evaporation cells. To this end, a special glass cell of Knudsen type was employed. This cell featured a diameter of about 10 mm with a 3 mm wide nozzle. Wiring of the resistive heating filament (0.5 mm thick Ta-wires) around the cell was done in different ways, either by focusing on the nozzle area (inset in Figure 5a) or on the backside of the cell (inset in Figure 5b). To discuss differences in the deposition behavior of this glass cell compared to a typical metal Knudsen cell, one needs to first recall the physical processes happening within such a cell. Clearly, the limited wiring of the heating filament, combined with the poor heat conductivity of quartz glass lead to a strongly varying temperature distribution along the long cell axis, contrary to

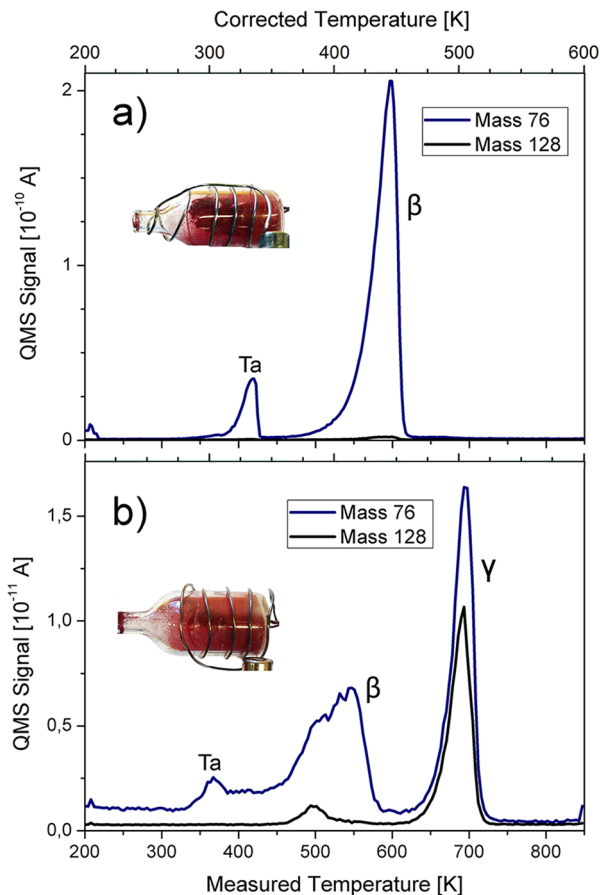


Figure 5. Thermal desorption spectra for quinacridone films deposited from a glass Knudsen-type cell with dense wiring near the nozzle (a) and after removal of said wiring and increased heating at the backside (b). The nominal film thicknesses are 5 nm in plot (a) and 2.5 nm in plot (b). Adsorption temperature: 200 K.

the required uniform heating of an ideal Knudsen source. In the first case, the nozzle area is, due to its smaller cross-section, significantly hotter than the residual cell walls. Due to the missing wiring at the backside we can, in turn, assume, that the back wall, where all the material leaving a Knudsen cell in a straight path typically comes from, is significantly colder in comparison and does therefore not contribute to any material deposition whatsoever. Instead, all molecules that eventually leave the cell in a direction where they can reach the sample surface need to have at least undergone one collision under low angle with the higher temperature cell wall in the nozzle area. Actually, the temperature of the nozzle is much higher than needed to just evaporate the material. Therefore, the thermally activated cracking process of quinacridone molecules can be expected to occur more likely in such an excessively hot nozzle. Indeed, deposition from a glass Knudsen cell featuring dense wiring near the nozzle area resulted in the complete cracking of every single quinacridone molecule, hence only the β -peak being visible in the TDS spectrum (Figure 5a). On the contrary, the usage of a glass Knudsen cell with a colder nozzle and a heated backside again showed partial cracking, comparable to results from a metal cell, and different molecular species were once again present on the sample (Figure 5b).

C. Surface Morphology. In order to take a closer look at the morphologies of the obtained films and for a possible morphological confirmation of the separate types of molecules

on the surface, we used ex-situ atomic force microscopy. All images were taken in tapping mode to not damage the sensitive organic films and plotted using derived data. In order to distinguish quinacridone islands from islands consisting of other molecules, it was necessary to create samples with either just quinacridone or just the decomposed molecules present. Samples with no quinacridone molecules adsorbed, i.e., samples with indigo and possible other decomposition products, were prepared by using the glass Knudsen cell described above with enhanced heating filament wiring near its opening (Figure 5a). Additionally, similar films were prepared via partial material desorption (β -peak) from one SiO_2 sample and subsequent adsorption onto another sample, as described above. Both methods produced comparable films and will therefore not be distinguished in the following. Moreover, all samples above a certain thickness that were produced by either of these methods displayed a deep blue color visible to the bare eye.

Pure quinacridone samples (with a bright pink color) could be manufactured by using the original metal Knudsen cell and heating the substrate to 425 K during the adsorption process, resulting in an immediate desorption of the weakly bonded smaller molecules. Figure 6 shows AFM images of three thick films on silicon dioxide with either all types of molecules (a), pure quinacridone (b) or solely indigo and other decomposed molecules (c) being present. All films did not show significant dewetting during venting (confirmed by TDS measurements) and Ostwald ripening or other morphology changes after storage under atmospheric conditions for at least 90 days, independent of molecule type and thickness. A comparison of surface morphologies for films of 5, 60, and 120 nm mean film thickness, as measured by AFM immediately after exposure to air and after 24 h, showed no changes in island size, shape, or number. This suggests that molecules within multilayer islands are immobile on the surface and show a stable configuration once they are incorporated into their respective bulk crystal structures.

Figure 6a shows a 42.5 nm thick film that was deposited from the metal Knudsen cell. Therefore, multiple types of molecules have been adsorbed and subsist on the surface. A multitude of islands is apparent, either round or slightly elongated, with heights up to 200 nm (cross-section Figure 6b). Samples grown from the special glass deposition cell or via substrate heating, as depicted in Figures 6c-e, show similarly shaped islands with comparable mean heights. Interestingly, for the pure films we could not observe the elongated islands as found for the mixed film. Initially we hoped to be able to correlate the two different island morphologies to the different types of molecules. While this might still be true, the different experimental conditions for the individual film fabrication (e.g., 425 K substrate temperature during quinacridone deposition, high nozzle temperature during indigo film preparation) might be responsible for this failure.

D. Structural Characterization. Quinacridone is a molecule with a planar conformation that crystallizes within the space group $P2_1/c$ with two molecules per unit cell. In the literature, up to seven different polymorph structures of linear trans-quinacridone have been reported.⁴²⁻⁵¹ However, only the β and γ -polymorphs (not to be mixed with the β and γ desorption peaks) are commercially important due to α -quinacridone transitioning either fully or partially into γ -quinacridone at elevated temperatures.^{39,52} From the crystal bulk structure it is apparent, that each molecule is connected to two neighboring molecules in the α and β -phase and to four

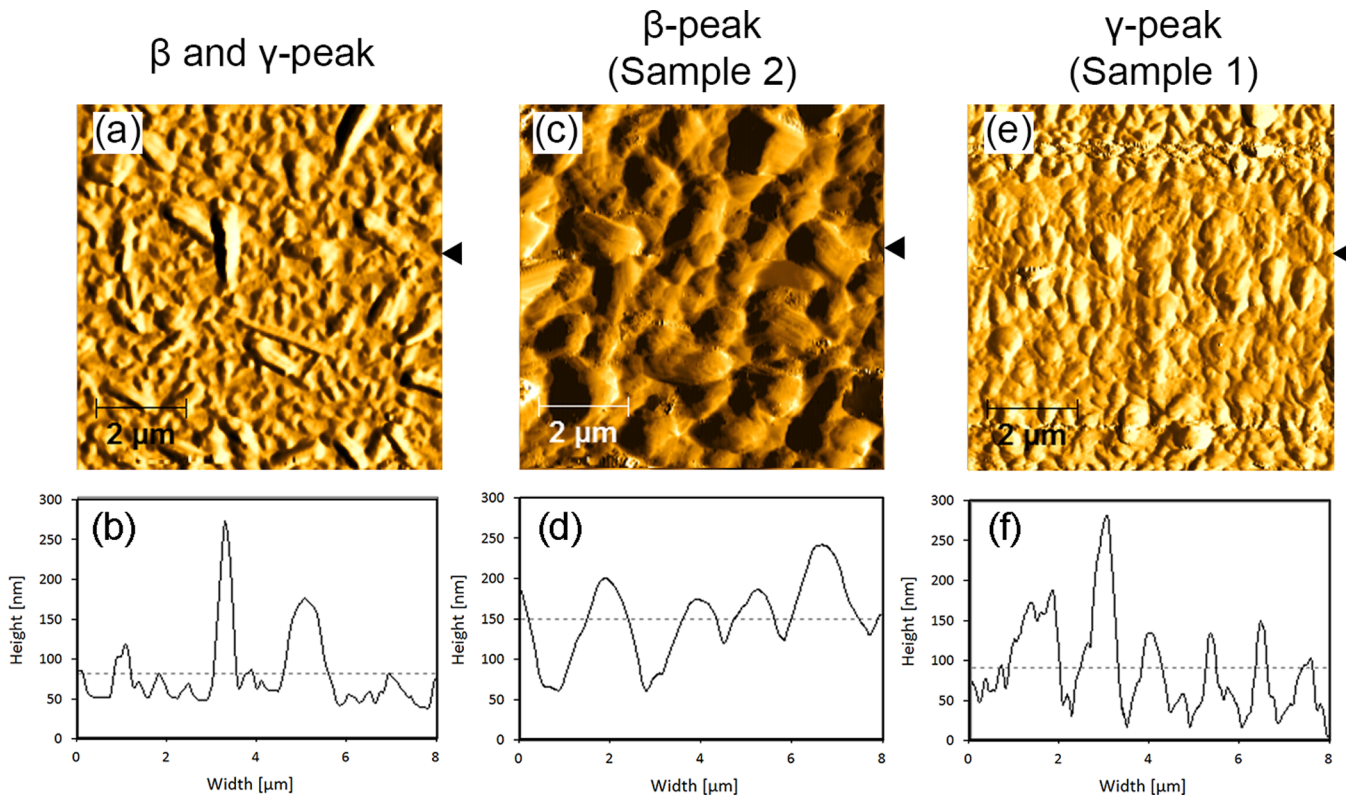


Figure 6. (a) AFM micrograph ($8 \mu\text{m} \times 8 \mu\text{m}$) of a quinacridone film containing additional cracking molecules on silicon dioxide deposited from a metal Knudsen cell at 200 K substrate temperature; nominal thickness: 42.5 nm. Deposition rate: 0.7 nm/min. (b) Cross section along the line marked by the black arrow in (a). (c) AFM micrograph ($8 \mu\text{m} \times 8 \mu\text{m}$) of a 85 nm thick film of the smaller cracking molecules, assumed to be mainly indigo, on silicon dioxide. The film was deposited from a glass Knudsen cell with enhanced heating near the opening; substrate deposition temperature: 200 K, deposition rate: 0.7 nm/min. (d) Cross section along the line marked by the black arrow in (c). (e) AFM micrograph ($8 \mu\text{m} \times 8 \mu\text{m}$) of a quinacridone film on silicon dioxide deposited from a metal Knudsen cell at a substrate temperature of 425 K. For this film, material equivalent to a nominal thickness of 170 nm was deposited onto the sample, but partial desorption caused the resulting layer to be significantly thinner (estimated thickness: 63 nm); deposition rate: 0.7 nm/min. (f) Cross section along the line marked by the black arrow in (e).

neighboring molecules in the γ -phase via intermolecular hydrogen bonds between the carbonyl and imino groups.⁵³ These comparatively strong bonds allow for a high thermal stability and a high melting point. Full crystallographic data of the bulk structure has only sparsely been published due to difficulties of crystal growth in solution and due to the typically insufficient quality of vapor deposited crystals.^{14,23,54}

In our own experiments we have investigated the crystallographic properties of two differently prepared films grown on SiO_2 with a thickness of 63 nm (sample 1) and 85 nm (sample 2), respectively, by using both specular and grazing-incidence X-ray diffraction. A specular scan of the first sample, grown from a metal Knudsen cell at a substrate temperature of 425 K, showed multiple out-of-plane reflections for scattering vectors q_z between 0.3 and 2.2 \AA^{-1} (Figure 7). A comparison with calculated diffraction data from powder cell measurements^{55,56} matches the peaks at 0.42 and 0.84 \AA^{-1} with (002) and (004) orientations of the quinacridone β -polymorph structure and peaks at 0.44 and 0.89 \AA^{-1} with (001) and (002) crystal orientations of the α -polymorph. Therefore, quinacridone molecules seem to exclusively arrange in crystallographic orientations where the (001) planes are parallel to the substrate. Figure 8 shows the packing of both the α and β crystallographic phases. Interestingly, there exist clear additional reflections which could not be attributed to any quinacridone net planes. Namely, reflections at 1.38, 1.42, and 1.63 \AA^{-1} are indications of the presence of p-sexiphenyl (6P, $\text{C}_{36}\text{H}_{26}$)⁵⁷ and/or other

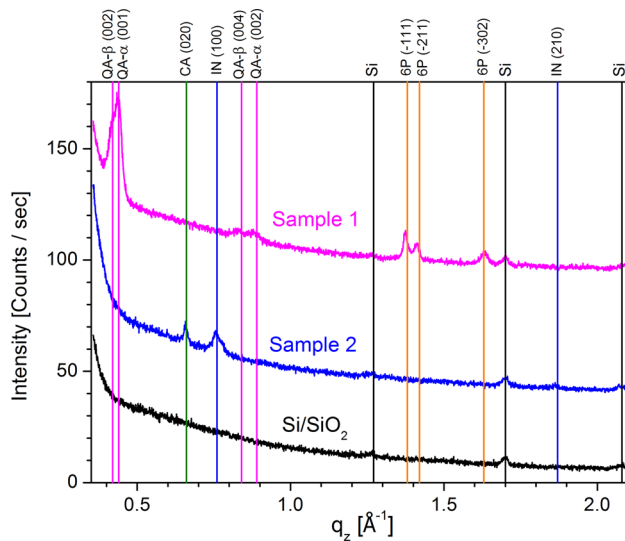


Figure 7. Specular X-ray diffraction pattern for a bare Si/SiO_2 substrate (black), a 63 nm thick quinacridone film with additional 6P reflections (sample 1, pink, compare to Figure 6e) and for a 85 nm thick film consisting of indigo and carbazole (sample 2, blue, compare to Figure 6c). Data are vertically shifted for better visibility.

oligophenylenes. However, there is no evidence of such molecules in the thermal desorption or mass spectra. We

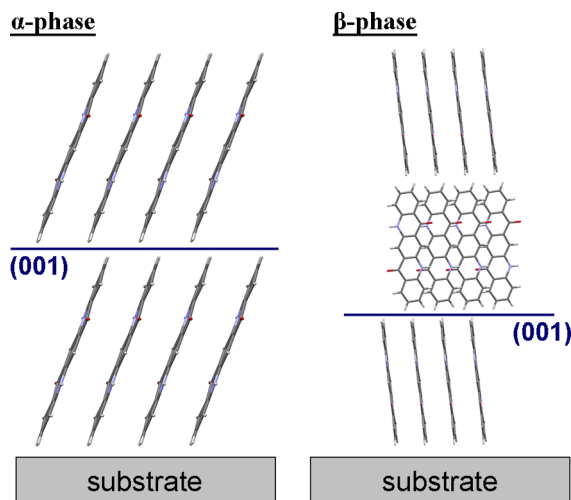


Figure 8. Preferred orientation of quinacridone molecules packing within the α - and β -polymorph with the (001)-planes parallel to the substrate.^{52,63}

believe that the occurrence of 6P is due to additional thermal decomposition and reaction of the impinging molecules at the relatively high substrate temperature of 425 K. During the growth process of this sample quinacridone molecules as well as all the described decomposition products in the Knudsen cell (indigo, carbazole) are present in the deposition flux. However, the latter cannot form a stable phase at a substrate temperature of 425 K and either instantly desorb or undergo further thermal decomposition. From a chemical point of view, both the break-off of CO and NH₃ molecules is quite likely, leading to a possible explanation of the formation of oligophenylenes from indigo, carbazole, and quinacridone molecules. The newly formed molecules have to be thermally stable on the surface at elevated temperatures, restricting the possible oligophenylenes to p-sexiphenyl and larger molecules.

Berg et al.²⁶ conducted similar experiments with 105 nm thick quinacridone films grown by vacuum sublimation on SiO₂ substrates. XRD peaks corresponding to α -(001), α -(002), β -(002), and β -(004) orientations were found, in accordance with our own experiments. In both phases molecules are orientated almost perpendicular to the substrate with their long axis tilted by only 10° and 20° with respect to the surface normal. Furthermore, it was shown that the relative peak distribution changes with increasing substrate temperature for the simple reason that the α -phase is metastable and that it can transform into a β -polymorph at elevated temperatures.⁵⁴ The α -polymorph was found to be favored for thin films with 11 nm nominal thickness. Therefore, we assign α to an interface-near substrate induced thin film phase while the β -polymorph is dominant within the bulk phase. Additionally, Sytnyk et al.¹⁵ recorded XRD patterns of quinacridone micro- and nanocrystals synthesized at various temperatures, and observed molecular arrangements that correspond to the α and β -polymorph throughout the measured temperature range.

The second film (sample 2) was prepared by using the special glass cell mentioned above with increased heating near the nozzle for the deposition process where desorption hinted at indigo. Indeed, a specular XRD scan (shown in Figure 7) clearly links the peaks at 0.76 and 1.87 Å⁻¹ to indigo corresponding to orientations where the (100) and (210) planes, respectively, are parallel to the substrate. Note that this

findings agree well with our recent work on indigo.²⁸ However, for this film again a special reflection appears in the XRD (0.66 Å⁻¹) which cannot be attributed to indigo. Extensive literature search showed that this reflection could be matched with a multitude of possible quinacridone cracking products,^{58–61} of which the (020) orientation of carbazole seems most likely if we take into account the entirety of the available spectroscopic data.

In order to provide support for the conclusions drawn from the specular X-ray diffraction data and to obtain additional information on the in-plane molecule arrangement we have carried out grazing incidence X-ray diffraction at BESSY II on the same samples as described before. Figure 9 shows two-dimensional GIXD images with an incidence wavelength of 1 Å and under an incidence angle of 0.13°. Numerous in-plane and out-of-plane reflections confirm the existence of a variety of

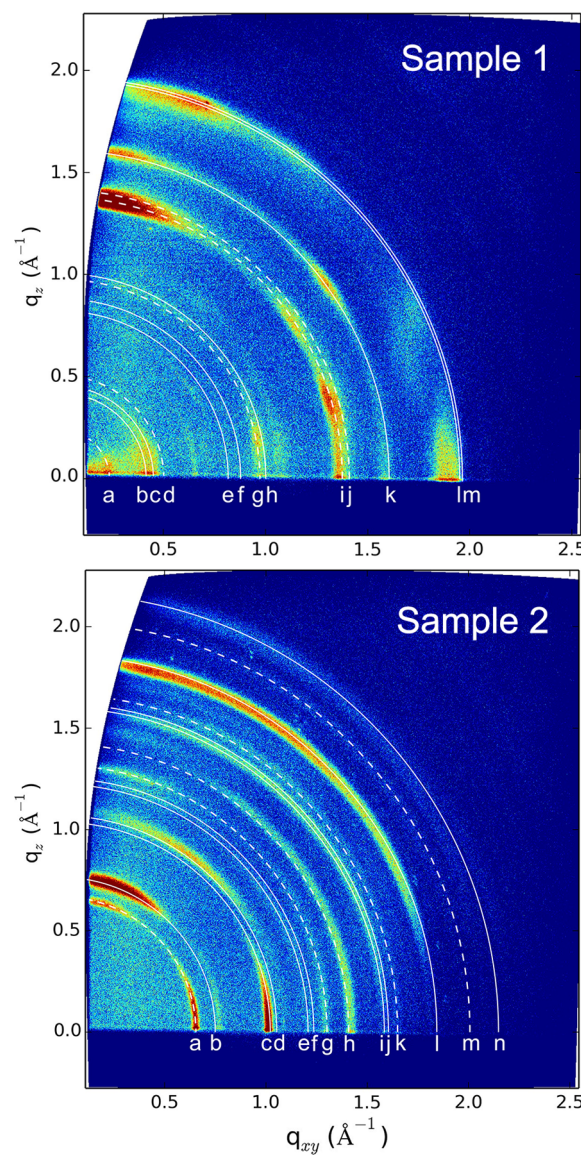


Figure 9. 2D-GIXD patterns of a 63 nm thick quinacridone film (sample 1, top) and a 85 nm film solely consisting of cracking molecules (sample 2, bottom). The white lines depict Debye-Scherrer rings of selected net planes of quinacridone (solid), p-sexiphenyl (dashed), indigo (solid), and carbazole (dashed); for detailed information see Table 1.

molecular species and additionally crystalline phases with different crystallographic orientations. The superimposed white lines represent the highest intensity reflections of quinacridone and p-sexiphenyl (top) as well as indigo and carbazole (bottom) taken from literature values (CSD-Codes QNACRD06, QNACRD07, ZZZNTQ01, INDIGO01, INDIGO02, and CRBZOL01).^{54,57,58,62,63} A detailed assignment list is given in Table 1.

Table 1. Crystallographic Reflections of *p*-Sexiphenyl, Quinacridone, Carbazole, and Indigo in Good Agreement with the Observed GIXD Reflection Spots

		q [\AA^{-1}]	molecule	phase	net plane (hkl)
sample 1	a	0.24	<i>p</i> -sexiphenyl		(100)
	b	0.42	quinacridone	β	(002)
	c	0.44	quinacridone	α	(001)
	d	0.48	<i>p</i> -sexiphenyl		(200)
	e	0.84	quinacridone	β	(004)
	f	0.89	quinacridone	α	(002)
	g	0.97	<i>p</i> -sexiphenyl		(400)
	h	1.00	quinacridone	α	(01-1)
	i	1.38	<i>p</i> -sexiphenyl		(-111)
	j	1.42	<i>p</i> -sexiphenyl		(-211)
	k	1.59	quinacridone	β	(011)
	l	1.95	quinacridone	β	(1-1-2)
	m	1.98	quinacridone	α	(1-12)
sample 2	a	0.66	carbazole		(020)
	b	0.76	indigo	A+B	(100)
	c	1.03	indigo	B	(-102)
	d	1.06	indigo	A	(-102)
	e	1.24	indigo	A	(011)
	f	1.26	indigo	B	(011)
	g	1.31	carbazole		(040)
	h	1.40	carbazole		(111)
	i	1.58	indigo	A	(111)
	j	1.61	indigo	B	(2-1-1)
	k	1.65	carbazole		(210)
	l	1.87	indigo	A+B	(210)
	m	1.98	carbazole		(211)
	n	2.15	indigo	A	(211)

E. Raman Spectroscopy. To interpret the results and features observed so far and for more information about the chemical composition of the thin organic films, Raman spectroscopy was employed on the two samples that were used for AFM, specular XRD and GIXD investigations before (compare Figures 6, 7, and 9). Both samples were irradiated with monochromatic light with a wavelength of 325 nm yielding a multitude of scattering peaks, as shown in Figure 10. We stress that the absolute peak intensities of the Raman modes in Figure 10 are arbitrary values that depend on the molecular orientations within the samples. We did not elaborate this finding in further detail, as our focus is here on a qualitative sample analysis. The quinacridone sample which was grown at a high substrate temperature (sample 1, pink) showed strong features at wavenumbers between 1550 and 1650 cm^{-1} and certain peaks in the area of 1350 cm^{-1} that agree reasonably well with our own powder measurements and literature values of quinacridone (see Figure 11 and Table 2).⁶⁴ Differences between thin film and powder measurements may, in this case, be explained by (a), the presence or dominant behavior of different polymorphs or (b), an increased amount

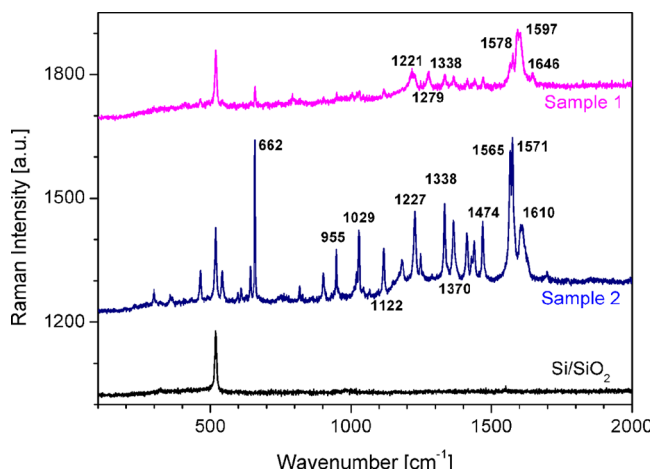


Figure 10. Raman spectra of a bare Si/SiO₂ substrate (black), a 63 nm thick quinacridone film (sample 1, pink), and a 85 nm thick film consisting of indigo and carbazole (sample 2, blue) upon irradiation with a wavelength of 325 nm.

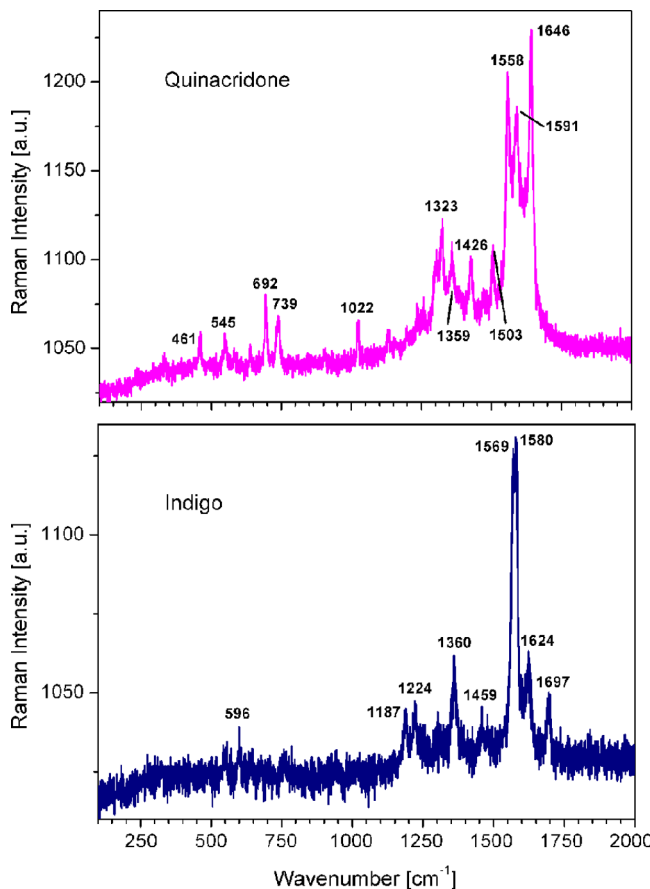


Figure 11. Raman spectra of quinacridone (pink) and indigo (blue) powder samples upon irradiation with a wavelength of 325 nm.

of intermolecular hydrogen bonds within the thin film compared to powder samples. Additional peaks at 1221 and 1279 cm^{-1} agree very well with p-sexiphenyl Raman excitations.⁶⁵ The second sample (sample 2, blue) shows a thoroughly different fingerprint with multiple excitations, due to no quinacridone but rather indigo and possible additional cracking molecules being present. Features at 1227, 1370, 1474, 1565, 1571, and 1610 cm^{-1} as well as additional smaller peaks,

Table 2. Observed 325 nm Excited Raman Features Compared with Powder Excitations of Indigo (IN) and Quinacridone (QA) and Possible Matches of the Remaining Features with Literature Data of *p*-Sexiphenyl (6P)⁶⁵ and Carbazole (CA)⁶⁶

	observed thin film Raman shift [cm ⁻¹]	observed powder Raman shift [cm ⁻¹]	closest Raman shift from lit. [cm ⁻¹]	molecule
sample 1	1221		1220	6P
	1279		1278	6P
	1338	1323		QA
	1578	1558		QA
	1597	1591	1594	QA/6P
	1646	1646		QA
sample 2	662		658	CA
	1029		1017	CA
	1122		1105	CA
	1227	1224	1226	IN/CA
	1338		1338	CA
	1370	1360		IN
	1474	1459	1483	IN/CA
	1565	1569		IN
	1571	1580	1575	IN/CA
	1610	1624	1629	IN/CA

can be matched with Raman excitations of indigo powder (see Figure 11 and Table 2). Certain peaks, most notably at 662, 1029, and 1122 cm⁻¹, are neither originating from quinacridone, nor from indigo vibrations, again corroborating our claim of the existence of at least one additional cracking molecule. They are in good agreement with carbazole literature data.⁶⁶

IV. CONCLUSIONS

In this work, we describe some idiosyncrasies in the context of the preparation of thin quinacridone films upon employing Knudsen cell deposition in ultrahigh vacuum. Since quinacridone exhibits a comparably high sublimation temperature, due to the existing hydrogen bonds, this causes partial decomposition in the Knudsen cell during evaporation, which impedes the formation of pure quinacridone films. We have used a variety of spectroscopies to unravel the thermally activated fragmentation and decomposition in the Knudsen cell by analyzing the effusion flux and the composition and structure of the deposited film. By using thermal desorption spectroscopy we could unambiguously demonstrate that at least two different species were deposited on a silicon dioxide substrate upon evaporation of quinacridone from a stainless steel Knudsen cell. In addition to quinacridone which desorbed at about 500 K (γ -peak), a second desorption peak (β -peak) appeared already at about 420 K, which could be attributed to indigo. With special experimental methods we were able to prepare films which exclusively consist of molecules corresponding to either the β -peak or the γ -peak, respectively. This was realized by desorbing and readsorbing molecules corresponding to the β or the γ -peak onto a second sample positioned opposite to the primary sample. Additionally, it was possible to prepare similar films with only one molecular species on the surface by either using a special Knudsen-like glass cell or by quinacridone deposition at elevated substrate temperatures. The latter films were subsequently analyzed by atomic force microscopy, specular X-ray diffraction, grazing-incidence X-ray diffraction, and Raman spectroscopy. These methods verified the existence of quinacridone and indigo in the respective samples. However,

additional decomposition products were found which could not be observed in the desorption spectra. In the film corresponding to the β -peak carbazole was detected in addition to indigo, while the film corresponding to the γ -peak displayed *p*-sexiphenyl, most likely created through further thermal decomposition processes at the hot substrate surface, in addition to quinacridone. These findings were supported by grazing-incidence and Raman spectroscopy. Pure quinacridone films could be prepared only upon using a Langmuir evaporation source (free evaporation). All films were stable and showed no significant morphology changes during venting and after storage in air for at least 90 days. Our study highlights that these findings are of relevance for choosing the proper deposition techniques for organic molecules with high sublimation temperature, in particular for hydrogen-bonded molecules, which attain increasing importance in the context of organic electronics.

■ AUTHOR INFORMATION

Corresponding Author

*Phone: +43 (316) 873–8463. E-mail: a.winkler@tugraz.at.

Author Contributions

The manuscript was written through contributions of all authors. All authors have given approval to the final version of the manuscript.

Notes

The authors declare no competing financial interest.

■ ACKNOWLEDGMENTS

We gratefully acknowledge the experienced support of Kurt Krenn (Karl Franzens Universität Graz, Institut für Erdwissenschaften, Bereich Mineralogie und Petrologie) for the Micro-Raman experiments. We would like to thank Prof. Schennach from Graz University of Technology for numerous fruitful discussions and helpful inputs. Additionally, we thank the Helmholtz Zentrum Berlin (HZB) for the allocation of synchrotron radiation beam time and gratefully acknowledge experimental support by Daniel Többens (HZB). This work was financially supported by the Austrian Science Fund FWF, Proj. No. P 23530 and TRP 239.

■ REFERENCES

- (1) Kaltenbrunner, M.; Sekitani, T.; Reeder, J.; Yokota, T.; Kuribara, K.; Tokuhara, T.; Drack, M.; Schwödauer, R.; Graz, I.; Bauer-Gogonea, S.; et al. An Ultra-Lightweight Design for Imperceptible Plastic Electronics. *Nature* **2013**, *499*, 458–463.
- (2) Kaltenbrunner, M.; White, M. S.; Glowacki, E. D.; Sekitani, T.; Someya, T.; Sariciftci, N. S.; Bauer, S. Ultrathin and Lightweight Organic Solar Cells with High Flexibility. *Nat. Commun.* **2012**, *3*, 770.
- (3) Sekitani, T.; Zschieschang, U.; Klauk, H.; Someya, T. Flexible Organic Transistors and Circuits with Extreme Bending Stability. *Nat. Mater.* **2010**, *9*, 1015–1022.
- (4) Forrest, S. R. The Path to Ubiquitous and Low-Cost Organic Electronic Appliances on Plastic. *Nature* **2004**, *428*, 911–918.
- (5) Glowacki, E. D.; Irimia-Vladu, M.; Bauer, S.; Sariciftci, N. S. Hydrogen-Bonds in Molecular Solids – from Biological Systems to Organic Electronics. *J. Mater. Chem. B* **2013**, *1*, 3742–3753.
- (6) Irimia-Vladu, M.; Troshin, P. A.; Reisinger, M.; Shmygleva, L.; Kanbur, Y.; Schwabegger, G.; Bodea, M.; Schwödauer, R.; Mumyatov, A.; Fergus, J. W.; et al. Biocompatible and Biodegradable Materials for Organic Field-Effect Transistors. *Adv. Funct. Mater.* **2010**, *20*, 4069–4076.
- (7) Smith, H. M. *High Performance Pigments*; Wiley-VCH: Weinheim, Germany, 2009.

- (8) Labana, S. S.; Labana, L. L. Quinacridones. *Chem. Rev.* **1967**, *67*, 1–18.
- (9) Liebermann, H.; Kirchhoff, H.; Glikman, W.; Loewy, L.; Gruhn, A.; Hammerich, T.; Anitschkoff, N.; Schulze, B. Über die Bildung von Chinakridonen aus p-Di-arylamino-terephthalsäuren. 6. Mitteilung über Umwandlungsprodukte des Succinylöbernsteinsäureesters. *Liebigs Ann. Chem.* **1935**, *518*, 245–259.
- (10) Pollak, P. New Routes in the Synthesis of Quinacridone Pigments. *Prog. Org. Coat.* **1977**, *5*, 245–253.
- (11) Schmidt, M. U.; Schmiermund, T.; Bolte, M. Disodium 2,5-bis(phenylamino)terephthalate decahydrate, an Intermediate in the Industrial Synthesis of Quinacridone Pigments. *Acta Crystallogr., Sect. C: Cryst. Struct. Commun.* **2006**, *62*, 37–40.
- (12) Johnson, R. U.S. Patent, 4197404A, 1978.
- (13) Urban, M. U.S. Patent, 5614014A, 1995.
- (14) Lincke, G. A Review of Thirty Years of Research on Quinacridones - X-ray Crystallography and Crystal Engineering. *Dyes Pigm.* **2000**, *44*, 101–122.
- (15) Sytnyk, M.; Glowacki, E. D.; Yakunin, S.; Voss, G.; Schöfberger, W.; Kriegner, D.; Stangl, J.; Trotta, R.; Gollner, C.; Tollabimazraehn, S.; et al. Hydrogen-Bonded Organic Semiconductor Micro- and Nanocrystals: From Colloidal Syntheses to (Opto-)Electronic Devices. *J. Am. Chem. Soc.* **2014**, *136*, 16522–16532.
- (16) Keller, U.; Müllen, K.; De Feyter, S.; de Schryver, F. C. Hydrogen-Bonding and Phase-Forming Behavior of a Soluble Quinacridone. *Adv. Mater.* **1996**, *8*, 490–493.
- (17) Javed, I.; Zhang, Z.; Peng, T.; Zhou, T.; Zhang, H.; Khan, M. I.; Liu, Y.; Wang, Y. Solution Processable Quinacridone Based Materials as Acceptor for Organic Heterojunction Solar Cells. *Sol. Energy Mater. Sol. Cells* **2011**, *95*, 2670–2676.
- (18) Chen, J. J.; Chen, T. L.; Kim, B.; Poulsen, D. A.; Mynar, J. L.; Fréchet, J. M. J.; Ma, B. Quinacridone-Based Molecular Donors for Solution Processed Bulk-Heterojunction Organic Solar Cells. *ACS Appl. Mater. Interfaces* **2010**, *2*, 2679–2686.
- (19) Jentzsch, T.; Juelpner, H. J.; Brzezinka, K.-W.; Lau, A. Efficiency of Optical Second Harmonic Generation from Pentacene Films of Different Morphology and Structure. *Thin Solid Films* **1998**, *315*, 273–280.
- (20) Athouel, L.; Froyer, G.; Riou, M. T.; Schott, M. Structural Studies of Parasexiphenyl Thin Films: Importance of the Deposition Parameters. *Thin Solid Films* **1996**, *274*, 35–45.
- (21) Zojer, E.; Koch, N.; Puschning, P.; Meghdadi, F.; Niko, A.; Resel, R.; Ambrosch-Draxl, C.; Knupfer, M.; Fink, J.; Brédas, J. L.; et al. Structure, Morphology, and Optical Properties of Highly Ordered Films of Para-sexiphenyl. *Phys. Rev. B: Condens. Matter Mater. Phys.* **2000**, *61*, 16538.
- (22) Locklin, J.; Roberts, M. E.; Mannsfeld, S. C. B.; Bao, Z. Optimizing the Thin Film Morphology of Organic Field-Effect Transistors: The Influence of Molecular Structure and Vacuum Deposition Parameters on Device Performance. *J. Macromol. Sci., Polym. Rev.* **2006**, *46*, 79–101.
- (23) Glowacki, E. D.; Irimia-Vladu, M.; Kaltenbrunner, M.; Gasiorowski, J.; White, M. S.; Monkowius, U.; Romanazzi, G.; Suranna, G. P.; Mastorilli, P.; Sekitani, T.; et al. Hydrogen-Bonded Semiconducting Pigments for Air-Stable Field-Effect Transistors. *Adv. Mater.* **2013**, *25*, 1563–1569.
- (24) Ruiz, R.; Choudhary, D.; Nickel, B.; Toccoli, T.; Chang, K.-C.; Mayer, A. C.; Clancy, P.; Blakely, J. M.; Headrick, R. L.; Iannotta, S.; et al. Pentacene Thin Film Growth. *Chem. Mater.* **2004**, *16*, 4497–4508.
- (25) Scherwitzl, B.; Lukesch, W.; Hirzer, A.; Albering, J.; Leising, G.; Resel, R.; Winkler, A. Initial Steps of Rubicene Film Growth on Silicon Dioxide. *J. Phys. Chem. C* **2013**, *117*, 4115–4123.
- (26) Berg, D.; Nielinger, C.; Mader, W.; Sokolowski, M. Quinacridone Organic Field Effect Transistors with Significant Stability by Vacuum Sublimation. *Synth. Met.* **2009**, *159*, 2599–2602.
- (27) Wagner, T.; Györök, M.; Huber, D.; Zeppenfeld, P.; Glowacki, E. D. Quinacridone on Ag(111): Hydrogen Bonding versus Chirality. *J. Phys. Chem. C* **2014**, *118*, 10911–10920.
- (28) Scherwitzl, B.; Resel, R.; Winkler, A. Film Growth, Adsorption and Desorption Kinetics of Indigo on SiO₂. *J. Chem. Phys.* **2014**, *140*, 184705.
- (29) Glowacki, E. D.; Romanazzi, G.; Yumusak, C.; Coskun, H.; Monkowius, U.; Voss, G.; Burian, M.; Lechner, R. T.; Demitri, N.; Redhammer, G. J.; et al. Epindolidiones—Versatile and Stable Hydrogen-Bonded Pigments for Organic Field-Effect Transistors and Light-Emitting Diodes. *Adv. Funct. Mater.* **2015**, *25*, 776–787.
- (30) Redhead, P. A. Thermal Desorption of Gases. *Vacuum* **1962**, *12*, 203–211.
- (31) Frank, P.; Hlawacek, G.; Lengyel, O.; Satka, A.; Teichert, C.; Resel, R.; Winkler, A. Influence of Surface Temperature and Surface Modifications on the Initial Layer Growth of Para-Hexaphenyl on Mica (001). *Surf. Sci.* **2007**, *601*, 2152.
- (32) Erko, A.; Packe, I.; Hellwig, C.; Sieber-Erdmann, M.; Pawlizki, O.; Veldkamp, M.; Gudat, W. KMC-2: The New X-Ray Beamline at BESSY II. *AIP Conf. Proc.* **2000**, *521*, 415–418.
- (33) Kriegner, D.; Wintersberger, E.; Stangl, J. Xray-Utilities: A Versatile Tool for Reciprocal Space Conversion of Scattering Data Recorded with Linear and Area Detectors. *J. Appl. Crystallogr.* **2013**, *46*, 1162–1170.
- (34) Japan AIST/NIMC Database Spectrum MS-NW-9353.
- (35) NIST Mass Spectrometry Data Center Spectrum MS-341442.
- (36) NIST Mass Spectrometry Data Center Spectrum MS-113349.
- (37) Puglisi, C.; Sturiale, L.; Montaudo, G. Thermal Decomposition Processes in Aromatic Polycarbonates Investigated by Mass Spectrometry. *Macromolecules* **1999**, *32*, 2194–2203.
- (38) Rice, F. O. The Thermal Decomposition of Organic Compounds from the Standpoint of Free Radicals I. - Saturated Hydrocarbons. *J. Am. Chem. Soc.* **1931**, *53*, 1959–1972.
- (39) Chung, F. H.; Scott, R. W. Vacuum Sublimation and Crystallography of Quinacridones. *J. Appl. Crystallogr.* **1971**, *4*, 506–511.
- (40) Haucke, G.; Graness, G. Thermal Isomerization of Indigo. *Angew. Chem., Int. Ed. Engl.* **1995**, *34*, 67–68.
- (41) Maissel, L. I.; Glang, R. *Handbook of Thin Film Technology*; McGraw Hill Book Company: New York, 1983.
- (42) Reidinger, A. D.; Struve, W. S. *Chem. Abstr.* **1959**, *53*, 1777d.
- (43) Struve, W. S. *Chem. Abstr.* **1959**, *53*, 1777f.
- (44) Manger, C. W.; Struve, W. S. *Chem. Abstr.* **1959**, *53*, 1777f.
- (45) Jaffe, E. E. Eur. Patent 305328, 1989.
- (46) Bäbler, F.; Jaffe, E. E. Eur. Patent 530143, 1993.
- (47) Tyson, R. S.; Schapiro, L. Ger. Patent 2435219, 1975.
- (48) Deusel, W.; Gundel, H. W.; Dauback, E. *Chem. Abstr.* **1963**, *59*, 14143e.
- (49) Schweizer, H. R. *Chem. Abstr.* **1969**, *70*, 30042.
- (50) Hashizume, K.; Miyatake, M.; Shigemitsu, M.; Kumano, I.; Katsura, H.; Ohshima, M. Br. Patent 1,243,652, 1968.
- (51) Wagener, A. P. *Chem. Abstr.* **1972**, *77*, 90071r.
- (52) Lincke, G.; Finzel, H.-U. Studies on the Structure of alpha-Quinacridone. *Cryst. Res. Technol.* **1996**, *31*, 441–452.
- (53) Fukunaga, H.; Fedorov, D. G.; Chiba, M.; Nii, K.; Kitaura, K. Theoretical Analysis of the Intermolecular Interaction Effects on the Excitation Energy of Organic Pigments: Solid State Quinacridone. *J. Phys. Chem. A* **2008**, *112*, 10887–10894.
- (54) Paulus, E. F.; Leusen, F. J. J.; Schmidt, M. U. Crystal Structures of Quinacridones. *CrystEngComm* **2007**, *9*, 131–143.
- (55) Panina, N.; Leusen, F. J. J.; Janssen, F. F. B. J.; Verwer, P.; Meekes, H.; Vlieg, E.; Derroover, G. Crystal Structure Prediction of Organic Pigments: Quinacridone as an Example. *J. Appl. Crystallogr.* **2007**, *40*, 105–114.
- (56) Cambridge Crystallographic Data Centre, 12 Union Road, 689 Cambridge CB2 1EZ, U.K.
- (57) Baker, K. N.; Fratini, A. V.; Resch, T.; Knachel, H. C.; Adams, W. W.; Soccia, E. P.; Farmer, B. L. Crystal Structures, Phase Transitions and Energy Calculations of Poly(p-Phenylene) Oligomers. *Polymer* **1993**, *34*, 1571–1587.

- (58) Kurahashi, M.; Fukuyo, M.; Shimada, A.; Furusaki, A.; Nitta, I. The Crystal and Molecular Structure of Carbazole. *Bull. Chem. Soc. Jpn.* **1969**, *42*, 2174–2179.
- (59) Dideberg, O.; Dupont, L.; André, J. M. The Crystal Structure of Dibenzofuran. *Acta Crystallogr., Sect. B: Struct. Crystallogr. Cryst. Chem.* **1972**, *28*, 1002–1007.
- (60) Rodriguez, M. A.; Bunge, S. D. Diphenylamine. *Acta Crystallogr., Sect. E: Struct. Rep. Online* **2003**, *59*, o1123–o1125.
- (61) Luss, H. R.; Smith, D. L. The Crystal and Molecular Structure of 9-Fluorenone. *Acta Crystallogr., Sect. B: Struct. Crystallogr. Cryst. Chem.* **1972**, *28*, 884–889.
- (62) Gribova, E. A.; Zhdanov, G. S.; Golder, G. A. X-Ray Determination of the Structure of Indigo and Thorindigo. *Kristallografiya* **1956**, *1*, 53–60.
- (63) Süss, P.; Wolf, A. A new Crystalline Phase of Indigo. *Naturwissenschaften* **1980**, *67*, 453.
- (64) Binant, C.; Guineau, B.; Lautie, A. Spectres de Vibration de Pigments Rouges de la Famille des Quinacridones. *Spectrochim. Acta* **1989**, *45*, 1279–1287.
- (65) Ohtsuka, H.; Furukawa, Y.; Tasumi, M. Dependencies of the Raman Spectra of p-Oligophenyls on the Chain Length and the Excitation Wavelength. *Spectrochim. Acta* **1993**, *49A*, 731–737.
- (66) Bree, A.; Zwarich, R. Vibrational Assignment of Carbazole from Infrared, Raman, and Fluorescence Spectra. *J. Chem. Phys.* **1968**, *49*, 3344–3355.